Advances in Brief

In Vivo Validation of 3′deoxy-3′-[^{18}F]fluorothymidine ([^{18}F]FLT) as a Proliferation Imaging Tracer in Humans: Correlation of [^{18}F]FLT Uptake by Positron Emission Tomography with Ki-67 Immunohistochemistry and Flow Cytometry in Human Lung Tumors[1]

Hubert Vesselle,[2] John Grierson, Mark Muzi, Jeffrey M. Pugsley, Rodney A. Schmidt, Peter Rabinowitz, Lanell M. Peterson, Eric Vallières, and Douglas E. Wood

Departments of Radiology (Division of Nuclear Medicine) [H. V., J. G., M. M., J. M. P., L. M. P.], Pathology [R. A. S., P. R.], and Surgery (Division of Thoracic Surgery) [E. V., D. E. W.], University of Washington, Seattle, Washington 98195

Abstract

Purpose: **Tumor proliferation has prognostic value in resected early stage non-small cell lung cancer (NSCLC) and can, therefore, predict which NSCLCs are at high risk for recurrence after resection and would benefit from additional therapy. It may also predict which tumor will respond to cell cycle-targeted chemotherapy and help assess the tumor response, besides helping to differentiate benign from malignant lung lesions. We evaluated whether the uptake of the new positron emission tomography (PET) tracer 3′deoxy-3′-[^{18}F]fluorothymidine (FLT) in a series of suspected NSCLCs correlated with tumor proliferation assessed by Ki-67 immunohistochemistry and flow cytometry.**

Experimental Design: **Ten patients with 11 biopsy-proven or clinically suspected NSCLC underwent 2-h dynamic PET imaging after i.v. injection of 0.07 mCi/kg FLT. Tumor FLT uptake was quantitated with the maximum pixel standardized uptake value (maxSUV), the partial volume corrected maxSUV (PV-corr-maxSUV), the average SUV over a small region-of-interest (aveSUV) and with Patlak analysis of FLT flux (aveFLTflux). The lesion diameter from computed tomography was used to correct the maxSUV for PV effects using recovery coefficients determined for the General Electric Advance PET scanner. Two of the 11 lesions were benign inflammatory lesions and 9 were NSCLCs. Immunohistochemistry for Ki-67 (proliferation index marker) was performed on all 11 tissue specimens (10 resections, 1 NSCLC percutaneous biopsy), and the S-phase fraction (SPF) from flow cytometry could be determined for 10. The specimens were reviewed for histology and cellular differentiation (poor, moderate, well). Lesions ranged from 1.6 to 7.7 cm.**

Results: **Excellent correlations were found between SUV measures of FLT uptake and Ki-67 scores [percentage of positive cells; maxSUV *versus* Ki-67: Rho = 0.78, $P = 0.0043$ ($n = 11$); PV-corr-maxSUV *versus* Ki-67: Rho = 0.83, $P = 0.0028$ ($n = 10$); aveSUV *versus* Ki-67: Rho = 0.84, $P = 0.0011$ ($n = 11$)]. Correlation between Ki-67 proliferation scores and Patlak measures of FLT uptake were also strong: aveFLTflux *versus* Ki-67: Rho = 0.94, $P < 0.0001$ ($n = 11$). The correlation between the SPF and all indices of FLT uptake was weaker and reached statistical significance for only two uptake indices [maxSUV *versus* SPF: Rho = 0.69, $P = 0.03$ ($n = 10$); PV-corr-maxSUV *versus* SPF: Rho = 0.36, $P = 0.35$ ($n = 9$); aveSUV *versus* SPF: Rho = 0.67, $P = 0.03$ ($n = 10$); aveFLTflux *versus* SPF: Rho = 0.46, $P = 0.18$ ($n = 10$)].**

Conclusion: **FLT PET may be used to noninvasively assess proliferation rates of lung masses *in vivo*. Therefore, FLT PET may play a significant role in the evaluation of indeterminate pulmonary lesions, in the prognostic assessment of resectable NSCLC, and possibly in the evaluation of NSCLC response to chemotherapy.**

Introduction

It is important to measure the proliferation rate of lung lesions to help differentiate benign from malignant tumors and to characterize malignant tumors. Tumor proliferation rate can predict which of the resectable NSCLCs[3] are at risk for recurrence after a complete presumably curative resection (1–17) and are, presumably, most likely to benefit from additional therapy, such as adjuvant or neo-adjuvant chemotherapy. Finally, the rate

Received 12/18/01; revised 6/28/02; accepted 7/19/02.
The costs of publication of this article were defrayed in part by the payment of page charges. This article must therefore be hereby marked *advertisement* in accordance with 18 U.S.C. Section 1734 solely to indicate this fact.
[1] Supported by NIH through National Cancer Institute Grant 1R01 CA80907.
[2] To whom requests for reprints should be addressed, at Department of Radiology, Division of Nuclear Medicine, Box 356113, University of Washington Medical Center, 1959 Northeast Pacific Street, Seattle, WA 98195. Phone: (206) 598-4240; Fax: (206) 598-4496; E-mail: vesselle@u.washington.edu.

[3] The abbreviations used are: NSCLC, non-small cell lung cancer; FLT, 3′deoxy-3′-[^{18}F]fluorothymidine (or radiolabeled FLT); SPF, S-phase fraction; ROI, region(s) of interest; GE, General Electric; SUV, standardized uptake value; maxSUV, maximum SUV; aveSUV, average tumor SUV; PV-corr-maxSUV, partial volume corrected maxSUV; CT, computed tomography; aveFLTflux, average FLT flux (into the tumor); PET, positron emission tomography; FDG, [F-18] fluorodeoxyglucose; TK1, thymidinekinase-1.

of proliferation of a NSCLC may predict its response to chemotherapeutic agents directed against dividing cells and may allow one to tailor NSCLC patients' therapy.

Present methods to assess tumor proliferation require a tissue sample and are, thus, limited by potential morbidity and sampling problems. A noninvasive method to assess proliferation might avoid unnecessary diagnostic biopsies of lung lesions and permit serial assessments during cancer therapy. Hence, extensive investigation has been made into evaluating tumor proliferation noninvasively by PET (18–24). Besides being noninvasive, PET imaging permits the evaluation of a tumor in its entirety, overcoming issues of heterogeneity and tumor sampling errors, and can easily be repeated at any point during treatment. Extensive work has been done at our institution and at others in the development and characterization of [^{11}C]thymidine for PET imaging (18–24). However, the short half-life of the ^{11}C label (20 min) together with the creation of labeled metabolites in the blood, which requires the use of compartment models for image interpretation, have limited the routine use of [^{11}C]thymidine PET imaging. To overcome these limitations, other potential tracers of proliferation such as 2′-[^{18}F]fluoro-5-methyl-1-β-D-arabinofuranosyluracil and [^{124}I]iododeoxyuridine have been investigated (25–28). Our group has investigated the radiotracer FLT (the abbreviation used for "3′-deoxy-3′-[18F]fluorothymidine" in this article; Refs. 29–34). FLT undergoes the same first metabolic step as thymidine and is monophosphorylated by thymidine kinase-1, an enzyme expressed during the DNA synthesis phase of the cell cycle (35–39). FLT monophosphate then accumulates in cells and is unable to cross the cell membrane (34). As a PET imaging tracer, FLT accumulates in cells as though it were incorporated into DNA (31, 36, 37, 40). Recent tumor cell studies performed at our institution have also demonstrated that when growth-arrested A549 human lung cancer cells were allowed to grow in fresh medium, FLT uptake in these cells increased steadily with times later than 6 h and correlated well with the percentage of cells in S phase ($r^2 = 0.91$; Ref. 32). On the basis of this lung cancer cell line evidence, we evaluated [^{18}F]FLT in human lung masses to explore its potential as a proliferation tracer for PET imaging. Our hypothesis was that the proliferation rate of human lung tumors as expressed by their Ki-67 immunohistochemistry score and SPF could be predicted *in vivo* by the accumulation of the radiolabeled FLT using PET (41).

Patients and Methods

Patient Selection

Ten patients with a total of 11 biopsy proven or clinically suspected NSCLCs were prospectively studied. These patients were initially evaluated in the Thoracic Surgery Clinic at the University of Washington Medical Center or the Veterans Affairs Puget Sound Health Care System between March 2000 and February 2001. All 11 of the lesions were considered potentially resectable. All of the patients had CT of the chest before FLT PET imaging. This study was conducted with University of Washington Human Subjects and Radiation Safety Committee-approved protocols.

FLT Synthesis

FLT was prepared according to the method developed by Grierson (29). FLT specific activity was greater than 1 Ci/μmol, decay corrected to the end of cyclotron bombardment. FLT was administered to patients by i.v. injection [10-ml solution of isotonic saline containing less than 10% (v/v) ethanol (USP)]. Calculation of doses was based on the patient's weight (0.07 mCi/kg), with a 5-mCi maximum dose. Before administration of each dose, quality control testing for pH (pH 7 ± 1) and radiochemical purity (>99%, high-performance liquid chromatography, thin-layer chromatography) was insured. All of the doses administered were also shown to be endotoxin free (<0.4 EU/ml, Limulus Amebocpe Lysis, Cape Cod Inc., Woods Hole, MA test). Sterility testing for anaerobic and aerobic bacterial contamination was performed on all of the batch dose samples, after radioactive decay (24 h).

FLT PET Imaging

Imaging. All of the PET studies were performed on a GE Advance PET Tomograph (GE Medical Systems, Waukesha, WI). FLT imaging was performed to quantitate FLT uptake as a proposed noninvasive measure of the primary tumor proliferation rate. No preparation was asked of the patients before tracer administration. After informed consent was obtained, two i.v. catheters or an i.v. and an intra-arterial catheter were placed in opposite arms. The tracer was administered through the first venous catheter, the other catheter (venous or radial arterial) was used for blood sampling. Arterial sampling was performed with an automated sampler described previously (42). Venous sampling was performed manually. Patients were placed supine in the scanner with the lung lesion and at least a portion of the left ventricular blood pool positioned to fit within the 15-cm wide tomograph field-of-view. Imaging started with a 20–25-min long transmission scan, performed over the selected field-of-view. Subsequently, a [F-18]FLT dose of 0.07mCi/kilogram of patient weight (not to exceed 5.0 mCi) was infused i.v. over one min using a Harvard pump (Harvard Clinical Technology, Inc., Boston, MA). A 2-h long dynamic emission scan was performed over the selected thoracic field-of-view starting 1 min before tracer infusion. Two separate dynamic imaging sequences were used: a single-field or a two-fields-of-view sequence. The imaging sequence for a single-field-of-view protocol was as follows: 8 15-s, 4 30-s, 6 1-min, 2 5-min, and 10 10-min imaging intervals. The imaging sequence for a two-fields-of-view (FOV1 and FOV2) protocol was as follows: FOV1: 4 25-s, 3 50-s, 3 2-min, and 10 5-min imaging intervals; FOV2: four 25-s, three 50-s, three 2-min, and nine 5-min imaging intervals. FOV1 and FOV2 imaging was interleaved from the start of imaging, and 15-s intervals were allowed for the table to move between the two fields-of-view. This allowed us to quantitate tracer uptake in the primary tumor (FOV1) and within another selected region (FOV2) for dosimetry studies.

All of the studies were collected in a two-dimensional imaging mode with scatter septae in place. Real-time randoms correction using counts obtained with a delayed coincidence window and deconvolution-based scatter corrections supplied by the manufacturer were applied. The raw PET data were reconstructed using the standard filtered back projection available on the GE Advance PET system. The following reconstruc-

Sphere Diam. (cm)	Maximum Pixel RC
3.3	1.01
2.8	1.01
2.2	0.88
1.6	0.57
1.2	0.38
1.0	0.26
0.8	0.16
0.6	0.08
0.4	0.01

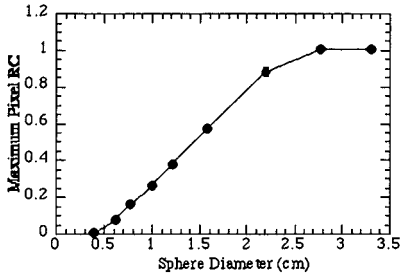

Fig. 1 Maximal pixel recovery coefficients calculated for spheres of known size and activity placed in a cold background. These spheres were imaged in the GE Advance PET scanner and the images reconstructed using the following parameters: 12-mm Hanning filter, 55-cm image diameter, and 128 × 128-array size. The maximal pixel recovery coefficient (*RC*) is equal to the measured maximal pixel activity (provided by the PET image) divided by the known activity present in the sphere.

tion parameters were used: 12-mm Hanning filter, 55-cm image diameter, and 128 × 128-array size.

Quantitative Imaging Analysis. Both the SUV and the FLT flux determined by Patlak analysis were used to quantitate tumor FLT uptake.

SUV. The SUV is defined as the time-averaged tissue activity *C* (μCi/ml), over an imaging time interval after injection, divided by the injected dose *ID* (mCi)/kg of patient body weight:

$$SUV = \frac{C\ (\text{mCi/ml})}{\dfrac{ID\ (\text{mCi})}{\text{Weight (kg)}}} \qquad \text{(A)}$$

C is the activity at a pixel within a tissue defined by a ROI. A tumor ROI (*ROI1*) encompassing the entire lesion was placed on all of the planes containing the lesion and applied to each of the dynamic image sets acquired between 30 and 60 min after tracer injection. For each pixel, the imaging data were summed up over the 30–60 min interval. The SUV value was computed for each pixel. Then, the pixel with the maxSUV within ROI1 was extracted (see "Results"). An additional ROI was also defined as containing all of the tumor pixels with values ≥50% of the maximum pixel value (ROI2). An aveSUV was defined by averaging the pixel SUV values within ROI2 for the images acquired between 30 and 60 min. We, therefore, investigated two separate definitions of the SUV: the maximum pixel SUV and an aveSUV over the 30–60 min imaging interval after FLT injection.

The maxSUV data were corrected for partial volume effects, based on the average diameter of the tumor (recovery coefficients). The average diameter of each lesion was calculated by averaging all three of the lesion dimensions measured from the mediastinal windows of the CT scan. The recovery coefficients have been estimated based on lesion diameter from phantom measurements performed in the GE Advance tomograph (43). These recovery coefficients (Fig. 1) have been calculated for the image reconstruction parameters and the filter used in imaging of NSCLC patients. These coefficients have been previously used by our group to correct the maximal pixel FDG-SUV of NSCLCs (44). For all of the lesions, these recovery coefficients (RC) were applied to the difference between lesion and normal lung background activities as defined by Eq. B. The aveSUV was not corrected for partial volume effects because of the difficulty in measuring the exact size of the ROI selected for averaging (ROI2) and the resulting inaccuracy in the recovery coefficient to be used.

The normal lung background, *i.e.*, the FLT uptake in normal lung, was evaluated over a large ROI placed away from the lung mass or nodule studied, and away from the chest wall and mediastinum. The aveSUV over this ROI was used as the background SUV. For lesions of diameter less than 2.8 cm, background FLT uptake contributes to the measured tumor uptake (Eq. B) because the recovery coefficient is less than 1 (Fig. 1).

$$\text{PV corrected maxSUV} = \text{Background SUV} + \frac{\text{Measured maxSUV} - \text{background SUV}}{\text{RC}} \qquad \text{(B)}$$

These implementations of the SUV were evaluated for correlation with the Ki-67 score and the SPF of lesions.

Patlak Analysis of FLT Flux. For each time frame of the dynamic imaging sequence, the pixels within ROI2 over the lesion were averaged, and the resulting set of dynamic values was analyzed by the graphical analysis method of Patlak *et al.* (45) to calculate the aveFLTflux. In this analysis, the tissue activity normalized to the FLT blood activity at each time point $[C_{tis}(t)/Cb_{FLT}(t)]$ is plotted against the normalized integral blood activity $[\int_0^t Cb_{total}/Cb_{FLT}(t)]$. The slope of the early linear portion of the curve (15–45 min) is an estimation of the flux of FLT.

Surgery and Pathology

Ten of 11 lung lesions were surgically resected after FLT PET imaging. One patient who had undergone a core biopsy of his primary NSCLC did not undergo a primary resection because a microscopic focus of tumor was discovered in a mediastinal lymph node at mediastinoscopy. He was instead administered neo-adjuvant chemoradiotherapy before subsequent resection. One patient had two histologically different primary NSCLCs resected, one from each lung and at two different surgeries. This patient's two lesions were imaged at the same time within a single PET field-of-view. Eleven histological specimens were available for pathological, immunohistochemical, and flow cytometric evaluation. All of the tumor specimens were reviewed by a pathologist (R. A. S.) to assess tumor type and differentiation (poor, moderate, or well-differentiated).

Ki-67 Immunohistochemistry. A representative formalin-fixed, paraffin-embedded section from each specimen was labeled using monoclonal antibody MIB-1 (Immunotech, Westbrook, ME; 1:100) after microwave antigen retrieval in citrate buffer. Antibody binding was detected using the Vectra Elite kit with FeCl3 intensification and hematoxylin counterstain. MIB-1 recognizes the Ki-67 antigen, a M_r 345,000 and 395,000 nuclear protein common to proliferating human cells (46). The fraction of labeled tumor cells (Ki-67 score) was assessed over a ×4 microscopic field (3-mm diameter) in the field that contained

Table 1 Summary of histological subtype and lesion differentiation, lesion average diameter, Ki-67 score, SPF, lesion aveSUV, maxSUV, PV-corr-maxSUV, and aveFLTflux measured for the 11 lesions evaluated

ID[a]	Patient	Histology	Lesion average diameter (cm)	Ki-67[b] (%)	SPF (%)	aveSUV (30–60 min)	maxSUV (30–60 min)	PV-corr-maxSUV (30–60 min)	aveFLTflux
1	WA	Benign inflammatory	3.9	2.5	1.6	0.91	0.90	0.90	0.82
2	PE	UD large cell carcinoma	1.6	90	1.6	3.40	4.02	6.82	5.44
3	RH	PD squamous cell carcinoma	2.47	70	49.3	4.09	5.86	6.22	4.89
4	CI	UD large cell carcinoma	5.5	90	19.4	5.39	6.90	6.90	6.25
5	GL	PD squamous cell carcinoma	2.07	20	13.3	2.46	2.56	3.05	1.97
6	CL	PD squamous cell carcinoma	7.66	60	0	1.91	2.32	[c]	2.01
7	CL	MD adenocarcinoma	2.57	60	6	2.80	3.77	3.92	2.59
8	SR	MD adenocarcinoma	1.73	30	1.6	3.28	4.26	6.41	2.85
9	WM	UD large cell carcinoma	3.7	70	2.6	4.29	5.60	5.60	5.16
10	CW	Benign inflammatory	1.97	2.5	0	0.76	1.42	1.75	1.78
11	PT	UD large cell carcinoma	2.5	80	[d]	3.53	4.64	4.89	3.88

[a] ID, identification; UD, undifferentiated; PD, poorly differentiated; MD, moderately differentiated.

[b] Ki-67 is defined: (*a*) in NSCLCs, as the percentage of tumor cells staining positive for MIB-1; (*b*) in benign lesions, as the percentage of all cells staining positive for MIB-1.

[c] Lesion 11 underwent a percutaneous core biopsy only, and, after immunohistochemical processing for Ki-67, insufficient tissue remained for flow cytometry.

[d] Lesion 6 was a large squamous cell carcinoma with a large area of central necrosis devoid of FLT uptake. For this reason and because the thickness of the tumor could not be measured, no partial volume correction was performed.

the highest average fraction of labeled cells. The pathologist scoring the immunohistochemical data (R. A. S.) was blinded to the FLT PET results. This same immunohistochemistry method was used and reported previously by our group (44).

Flow Cytometry. To provide for a meaningful comparison of SPF and Ki-67 scores, the area of a tumor selected and scored for Ki-67 immunohistochemistry was marked on the MIB-1 stained slide. This mark was then used to orient the paraffin tumor block so that two 60-μm thick slices of the block could be recut for processing by the flow cytometry laboratory (P. R.). This slice thickness was selected to provide enough nuclei for this analysis. The nuclei of the two slices corresponding to the area marked on the immunohistochemistry slide were evaluated by flow cytometry. An attempt was made to stain the sample with a cytokeratin-specific antibody to selectively evaluate the epithelial component of the tumor. The SPF of the lesion was determined by cytokeratin-gated flow cytometry on all cellular components of the sample. All of the flow cytometry data were reviewed by a pathologist specialized in interpreting them (P. R.).

Statistical Analysis

Because the Ki-67 scores and SPFs are values ranging between 0 and 100%, and not normally distributed, the nonparametric Spearman rank test was used to evaluate their correlation with tumor FLT uptake.

Results

Data for the 11 lesions evaluated in this study are summarized in Table 1. Fig. 2 illustrates the relative uptake at FLT PET imaging of four representative lesions spanning the range of proliferation rates.

The 11 lesions ranged in size from 1.6 cm to 7.7 cm. Two lesions were found to be benign inflammatory nodules at frozen-section performed at the time of stapled wedge resection. The other nine lesions were NSCLCs: three squamous cell carcinomas, four large cell carcinomas and two adenocarcinomas. For all of the tumors except one large lesion with central necrosis, the average lesion diameter was determined from CT scans and the corresponding recovery coefficient was applied to the lesion maxSUV while accounting for normal lung uptake (Eq. B). For the 11th lesion, FLT uptake was present within the wall of this lesion but not within the necrotic center, and conventional imaging did not allow determination of the thickness of the wall for partial volume correction.

Ki-67 scores, the percentage of cells positive for the MIB-1 antibody, were measured for all 11 lesion specimens. A strong correlation is found between all three SUV-based definitions of FLT uptake (maxSUV, PV-corr-maxSUV, aveSUV) and the Ki-67 score of lesions (Figs. 3, 4, and 5): maxSUV *versus* Ki-67: Rho = 0.78, $P = 0.0043$ ($n = 11$); PV-corr-maxSUV *versus* Ki-67: Rho = 0.83, $P = 0.0028$ ($n = 10$); aveSUV *versus* Ki-67: Rho = 0.84, $P = 0.0011$ ($n = 11$).

The Patlak-derived FLT flux into lesions (aveFLTflux) shows an even stronger correlation with Ki-67 scores ($n = 11$): aveFLTflux *versus* Ki-67: Rho = 0.94, $P < 0.0001$ (Fig. 6).

If the FLT uptake of the nine NSCLCs is analyzed in the absence of the two benign inflammatory lesions, we find the after results: maxSUV *versus* Ki-67: Rho = 0.61, $P = 0.08$ ($n = 9$ NSCLCs); PV-corr-maxSUV *versus* Ki-67: Rho = 0.67, $P = 0.07$ ($n = 8$ NSCLCs); aveSUV *versus* Ki-67: Rho = 0.72, $P = 0.03$ ($n = 9$ NSCLCs); aveFLTflux *versus* Ki-67: Rho = 0.89, $P = 0.0015$ ($n = 9$ NSCLCs).

Cytokeratin-gated flow cytometry was attempted on all of the specimens, but only two of them resulted in a positive stain with the ability of gating the SPF calculation on the epithelial population of

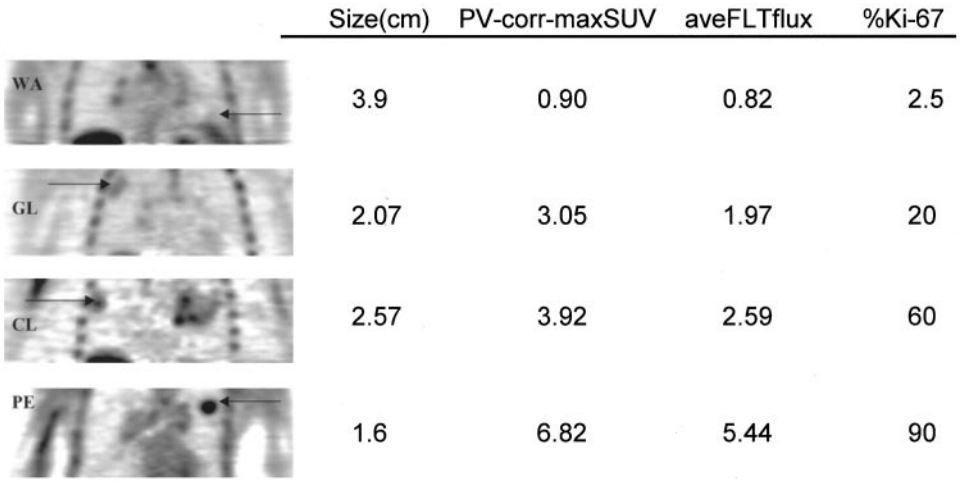

Fig. 2 This figure illustrates the FLT PET imaging appearance of lesions with different proliferation rates. A benign lesion and three NSCLCs with, respectively, low, intermediate, and high Ki-67 scores are represented, and the lesion FLT uptake values are cross-referenced.

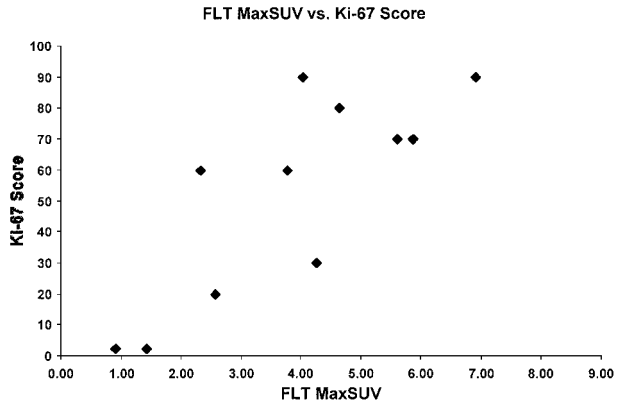

Fig. 3 Relationship between the FLT maxSUV and the Ki-67 score of the lung lesions [Rho = 0.78, $P = 0.0043$ ($n = 11$)].

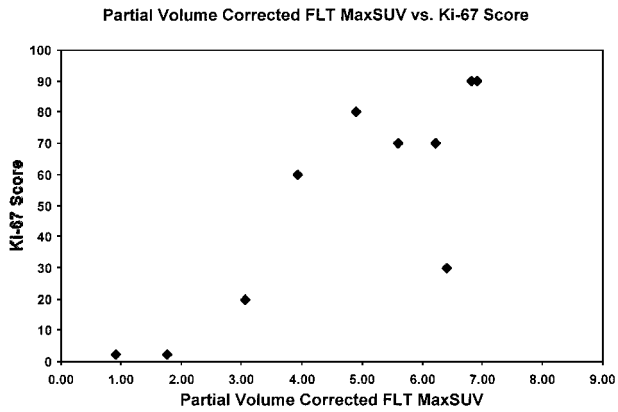

Fig. 4 Relationship between the PV-corr-maxSUV and the Ki-67 score of the lung lesions [Rho = 0.83, $P = 0.0028$ ($n = 10$)].

cells within each lesion. The results reported here represent the SPF of all of the cells within the lung tumors. One specimen obtained by core biopsy provided insufficient material left for flow cytometry after Ki-67 processing of the tissue block. Therefore, only 10 lesions had SPF determination. The correlations between the SPF and all of the indices of FLT uptake were weaker and reached statistical significance for only two uptake indices: maxSUV *versus* SPF: Rho = 0.69, $P = 0.03$, ($n = 10$); PV-corr-maxSUV *versus* SPF: Rho = 0.36, $P = 0.35$, ($n = 9$); aveSUV *versus* SPF: Rho = 0.67, $P = 0.03$, ($n = 10$); aveFLTflux *versus* SPF: Rho = 0.46, $P = 0.18$, ($n = 10$).

A modest correlation that did not reach statistical significance was found between Ki-67 scores and SPFs: Rho = 0.45, $P = 0.19$, $n = 10$.

No statistically significant correlation was found between tumor size and Ki-67 score (Rho = 0.07, $P = 0.83$, $n = 11$ lesions) or SPF of the tumor (Rho = 0.098, $P = 0.79$, $n = 10$ lesions).

Discussion

Previously reported PET imaging studies of FLT have involved static imaging and reports of FLT SUV values compared with FDG SUV values as well as descriptive reports of FLT image appearance (31, 47–50). However, the relationship between *in vivo* human tumor FLT uptake and tissue proliferation indices has not been investigated yet. The results reported here from a series of 11 lung lesions indicate that FLT uptake (quantitated either as aveSUVs or maxSUVs or as Patlak FLT flux) correlates strongly with lesion cellular proliferation assessed by Ki-67 immunohistochemistry (41) and to a lesser extent with lesion SPF.

Static (SUV) and dynamic (Patlak flux) imaging measures of tumor FLT uptake were assessed in this study. These methods differ greatly in the complexity of their data acquisition and analysis. We evaluated tumors with 2-h long dynamic imaging to compare simple static SUV measures of FLT uptake with the more complicated FLT flux determination in their potential correlation with tissue proliferation markers. We evaluated FLT uptake from static imaging data (SUV) for the following reasons: (*a*) for FLT uptake to have widespread clinical application as a noninvasive means of grading tumor proliferation, it needs to be easy to perform without requiring dynamic imaging; (*b*) shorter imaging protocols for SUV static imaging help

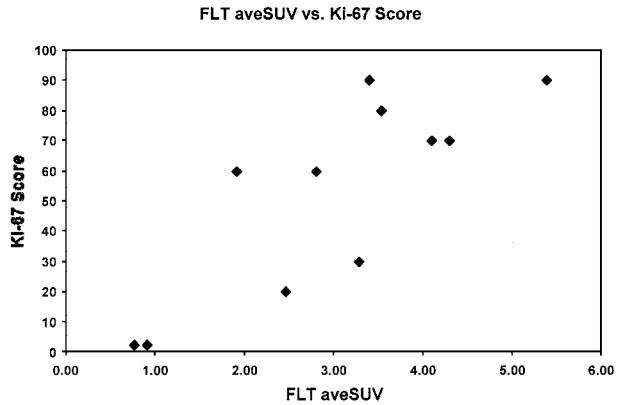

Fig. 5 Relationship between the FLT aveSUV and the Ki-67 score of the lung lesions [(Rho = 0.84, $P = 0.0011$ ($n = 11$)].

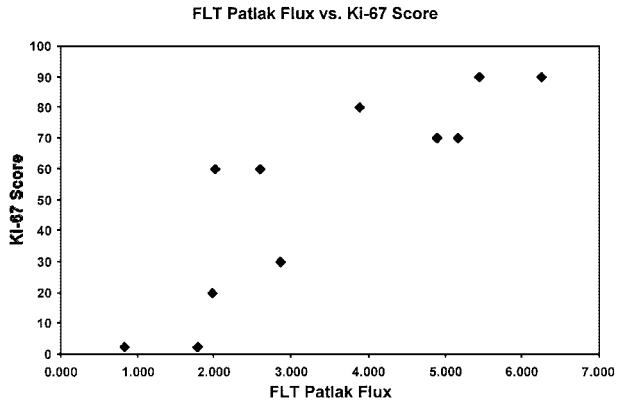

Fig. 6 Relationship between the aveFLTflux (*FLT Patlak Flux*) and the Ki-67 score of the lung lesions [Rho = 0.94, $P < 0.0001$ ($n = 11$)].

maximize patient enrollment and compliance with the imaging protocol. We also quantitated FLT uptake with a Patlak determination of FLT flux from complete dynamic data to assess the incremental benefit gained from a more extensive imaging and analysis approach.

Tumor proliferative rates may be estimated in human tumor samples by mitotic figure counting, immunohistochemical detection of cell cycle-specific proteins (Ki-67 and PCNA), and the SPF determination from DNA flow cytometry. However, mitotic figure counting is affected by interobserver reproducibility problems, use of mitotic indices *versus* mitoses per area, time between tumor resection and fixation, and the laborious nature of the analysis. The staining process for proliferating cell nuclear antigen with the PC10 antibody has the disadvantages of being sensitive to variations in the fixation technique, and, moreover, the microwave treatment in the staining process can cause nonproliferating cells to become stained (51, 52). In addition, the PCNA protein has a long half-life in cells and can be present after the proliferation phase has been completed (53). Consequently, quiescent cells can stain positive for PCNA.

Evaluating the expression of the Ki-67 protein in cells can also assess cell proliferation. Ki-67 is a protein expressed only in proliferating cells. The protein is present in the S phase and in G_2 and M phases of the cell cycle, as well as in the proliferation-associated part of G_1, but not in G_0 (54). Ki-67 has been shown to be required for cellular proliferation (55), to be synthesized as a cell begins proliferation, and to be efficiently degraded at the end of the proliferative cycle (reviewed in Ref. 56). Ki-67 protein expression is strictly correlated with cell proliferation and with the active phases of the cell cycle (56). Dependent on the cell proliferation cycle phase, the cellular level of the Ki-67 protein varies; however, detection by an antibody to Ki-67 is possible during the entire life of the protein. Cellular proliferation assessment with Ki-67 measures a tumor-growth parameter that is distinct from both PCNA and flow cytometry (57). Two antibodies against the Ki-67 protein, the Ki-67 antibody and MIB-1, are available for use in immunohistochemical assays. MIB-1 is a more recent discovery and can be used with formalin-fixed paraffin-embedded tissue sections, whereas the Ki-67 antibody can be used only with fresh or frozen tissue (58). Thus, MIB-1 is more versatile because fresh tissue is not available for retrospective studies and because paraffin embedding is the most common tissue preservation technique used in clinical settings. The selection of the Ki-67 marker as a tissue correlate for tumor FLT uptake was made in consideration of: (*a*) the versatility of the MIB-1 antibody; (*b*) the inherent limitations of the mitotic index and PCNA; (*c*) the ease with which expression of cell cycle-specific proteins, such as the Ki-67-related antigen, can be assessed semiquantitatively. Another argument for selecting the Ki-67 proliferation score is that it has been shown to have prognostic significance in NSCLC and several other tumor types as reviewed by Scholzen and Gerdes (56). We found excellent correlations between all of the indices of FLT uptake that we calculated and the Ki-67 score of tumors assessed by MIB-1 immunohistochemistry.

DNA flow cytometry is complicated by technical difficulties in obtaining nuclei for analysis, multiple cell populations in the tumor sample in which the cell cycle compartments may be inextricably intermixed, and various methods for calculating SPFs. However, SPF is a well-accepted standard in cell culture experiments, and such experiments performed at our institution have revealed a correlation between FLT uptake and SPF in A549 human lung cancer cells (32). Another group recently reported a correlation between FLT uptake of several asynchronously growing human tumor cell lines and their SPFs (59). As stated above, flow cytometry measures a tumor growth parameter that is distinct from Ki-67 (57). For these reasons, we also evaluated tumor proliferation using flow cytometry. When compared with the strong correlations found between FLT uptake and Ki-67 scores, we found more modest correlations between indices of FLT uptake and the SPF. The lack of statistical significance in the correlation between the SPF and the PV-corr-maxSUV or the FLT flux likely stems from the more limited number of samples. The correlation between SPF and FLT uptake is probably weaker because, contrary to the Ki-67 antigen, the SPF describes cells only in S phase, rather than the total non-G_0 compartment. It is known that the uptake of FLT is tightly linked to TK1 enzyme activity (33). In cycling cells, TK1 expression increases in late G_1, then significantly increases

throughout S phase and G2, reaching maximum levels during mitosis (60). Therefore, the SPF is unlikely to be an optimal proliferation index for correlation with TK1 activity or FLT uptake. This is corroborated by the results of Rasey *et al.* (33) who showed that growth-arrested A549 cells stimulated to grow in fresh medium, demonstrated increased FLT uptake and increased TK1 activity with essentially no movement of cells from G_1 into S phase after 12–14 h. This was reported to be consistent with an increase in TK1 activity in late G_1 before DNA synthesis and is also consistent with a slightly better correlation of FLT uptake with TK1 activity than with SPF. In their study, FLT uptake, TK1 activity, and SPF peaked by 24–28 h. In other words, in a cell population, FLT uptake may be indicative of cells preparing to divide as well as of cells dividing and of cells synthesizing DNA.

Human solid tumors are composed of asynchronous cell populations, and the determination of an SPF in such cell lines may underestimate the percentage of cells involved in proliferation. In addition, the temporal relationship between TK1 expression and SPF may vary between the different cell lines contributing to a weaker correlation of FLT uptake with SPF.

A modest correlation was found between the Ki-67 score and SPF of the lesions in our series (Rho = 0.45, $P = 0.19$). This is in keeping with the correlations reported in the literature for different proliferation indices.

With four different methods of evaluating FLT uptake (maxSUV, PV-corr-maxSUV, aveSUV, and aveFLTflux) we found a strong correlation between FLT uptake and the Ki-67 score. This suggests that the correlation between FLT uptake and the Ki-67 proliferative index is robust.

No statistically significant correlation was found in our series between the size of a lesion and its Ki-67 score or SPF. This would be expected because the size of a lesion represents a single time point measurement during its growth and does not reflect its growth rate as a proliferation score can.

In conclusion, this preliminary investigation demonstrates that FLT uptake in lung lesions correlates with the proliferation rate of such lesions assessed by Ki-67 immunohistochemistry and to a lesser extent with their SPF. This was demonstrated after quantifying FLT uptake either with simple static imaging uptake indices, such as SUVs over 30–60 min, or with more elaborate uptake values such as the FLT flux determined from a Patlak analysis of dynamic imaging data.

The correlation between FLT uptake of lung lesions and their proliferation rate has important clinical implications for PET imaging and characterization of lung lesions. FLT PET imaging could be used to differentiate benign from malignant lung lesions on the basis of their FLT uptake and, therefore, growth rate because most benign lung lesions do not proliferate. This will necessitate further validation with a large series of benign lesions. In addition, the prognostic significance of Ki-67 in NSCLC suggests that FLT uptake could be used to refine the prognostic assessment of NSCLCs. Finally, because NSCLCs with high Ki-67 scores are at higher risk for recurrence after resection, preoperative FLT uptake determination could be used to select which patients would benefit from additional therapy such as neo-adjuvant or adjuvant chemotherapy. Moreover, FLT uptake may help to assess the effects on tumors of therapies targeted at the cell cycle. These encouraging results are, therefore, opening the door to further evaluation and validation of FLT PET imaging.

Acknowledgments

We thank Drs. Janet Eary and Satoshi Minoshima for helpful comments, the University of Washington Medical Center technologists, and the University of Washington PET physics group for their technical support.

References

1. Harpole, D. J., Herndon, J. E., II, Wolfe, W. G., Inglehart, J. D., and Marks, J. R. A prognostic model of recurrence and death in stage I non-small cell lung cancer utilizing presentation, histopathology, and oncoprotein expression. Cancer Res., *55:* 51–56, 1995.

2. Macchiarini, P., Fontanini, G., Hardin, M., Chuanchieh, H., Bigini, D., Vignati, S., Pingitore, R., and Angeletti, C. A. Blood vessel invasion by tumor cells predicts recurrence in completely resected T_1 N_0 M_0 non-small-cell lung cancer. J. Thorac. Cardiovasc. Surg., *106:* 80–89, 1993.

3. Takise, A., Kodama, T., Shimosato, Y., Watanabe, S., and Suemasu, K. Histopathologic prognostic factors in adenocarcinomas of the peripheral lung less than 2 cm in diameter. Cancer (Phila.), *61:* 2083–2088, 1988.

4. Dazzi, H., Thacher, N., Hasleton, P., Chatterjee, A., and Lawson, R. DNA analysis by flow cytometry in nonsmall cell lung cancer: relationship to epidermal growth factor receptor, histology, tumour stage and survival. Respir. Med., *84:* 217–223, 1990.

5. Filderman, A., Silvestri, G., Gatsonis, C., Luthringer, D., Honig, J., and Flynn, S. Prognostic significance of tumor proliferative fraction and DNA content in stage I non-small cell lung cancer. Am. Rev. Respir. Dis., *146:* 707–710, 1992.

6. tenVelde, G., Schutte, B., Vermeulen, A., Volovics, A., Reynders, M., and Blijham, G. Flow cytometric analysis of DNA ploidy level in paraffin-embedded tissue of non-small-cell lung cancer. Eur. J. Cancer Clin. Oncol., *24:* 455–460, 1988.

7. Volm, M., Hahn, E., Mattern, J., Muller, T., Vogt-Moykopf, I., and Weber, E. Five-year follow-up study of independent clinical and flow cytometric prognostic factors for the survival of patients with non-small cell lung carcinoma. Cancer Res., *48:* 2923–2928, 1988.

8. Ishida, T., Kaneko, S., Akazawa, K., Tateishi, M., Sugio, K., and Sugimachi, K. Proliferating cell nuclear antigen expression and argyrophilic nucleolar organizer regions as factors influencing prognosis of surgically treated lung cancer patients. Cancer Res., *53:* 5000–5003, 1988.

9. Ebina, M., Steinberg, S., Mulshine, J., and Linnoila, R. Relationship of p53 overexpression and up-regulation of proliferating cell nuclear antigen with the clinical course of non-small cell lung cancer. Cancer Res., *54:* 2496–2503, 1988.

10. Fontanini, G., Macchiarini, P., Pepe, S., Ruggiero, A., Hardin, M., Bigini, D., Vignati, S., Pingitore, R., and Angeletti, C. A. The expression of proliferating cell nuclear antigen in paraffin sections of peripheral, node-negative non-small cell lung cancer. Cancer (Phila.), *70:* 1520–1527, 1992.

11. Macchiarini, P., Fontanini, G., Hardin, M., Squartini, F., and Angeletti, C. Relation of neovascularisation to metastasis of non-small-cell lung cancer. Lancet, *340:* 145–146, 1992.

12. Hommura, F., Dosaka-Akita, H., Mishina, T., Nishi, M., Kojima, T., Hiroumi, H., Ogura, S., Shimizu, M., Katoh, H., and Kawakami, Y. Prognostic significance of p27KIP1 protein and ki-67 growth fraction in non-small cell lung cancers. Clin. Cancer Res., *6:* 4073–4081, 2000.

13. Komaki, R., Milas, L., Ro, J. Y., Fujii, T., Perkins, P., Allen, P., Sikes, C. R., Mountain, C. F., and Ordonez, N. G. Prognostic biomarker study in pathologically staged N_1 non-small cell lung cancer. Int. J. Radiat. Oncol. Biol. Phys., *40:* 787–796, 1998.

14. Puglisi, F., Aprile, G., Bruckbauer, M., Barbone, F., Damante, G., Guerra, S., Beltrami, C. A., and Di Loreto, C. Combined analysis of

MIB-1 and thyroid transcription factor-1 predicts survival in non-small cell lung carcinomas. Cancer Lett., *162:* 97–103, 2001.

15. Mehdi, S., Etzell, J., Newman, N., Weidner, N., Kohman, L., and Graziano, S. Prognostic significance of Ki-67 immunostaining and symptoms in resected stage I and II non-small cell lung cancer. Lung Cancer, *20:* 99–108, 1998.

16. Pence, J., Kerns, B., Dodge, R., and Igelhart, J. Prognostic significance of the proliferation index in surgically resected non-small-cell lung cancer. Arch. Surg., *128:* 1382–1390, 1993.

17. Shiba, M., Kohno, H., Kakizawa, K., Iizasa, T., Otsuji, M., Saitoh, Y., Hiroshima, K., Ohwada, H., and Fujisawa, T. Ki-67 immunostaining and other prognostic factors including tobacco smoking in patients with resected nonsmall cell lung carcinoma. Cancer (Phila.), *89:* 1457–1465, 2000.

18. Eary, J. F., Mankoff, D. A., Spence, A. M., Berger, M. S., Olshen, A., Link, J. M., O'Sullivan, F., and Krohn, K. A. 2-[^{11}C]Thymidine imaging of malignant brain tumors. Cancer Res., *59:* 615–621, 1999.

19. Mankoff, D. A., Shields, A. F., Graham, M. M., Link, J. M., Eary, J. F., and Krohn, K. A. Kinetic analysis of 2-[carbon-11]thymidine PET imaging studies: compartmental model and mathematical analysis. J. Nucl. Med., *39:* 1043–1055, 1998.

20. Mankoff, D. A., Shields, A. F., Link, J. M., Graham, M. M., Muzi, M., Peterson, L. M., Eary, J. F., and Krohn, K. A. Kinetic analysis of 2-[^{11}C]thymidine PET imaging studies: validation studies. J. Nucl. Med., *40:* 614–624, 1999.

21. Martiat, P., Ferrant, A., Labar, D., Cogneau, M., Bol, A., Michel, C., Michaux, J. L., and Sokal, G. *In vivo* measurement of carbon-11 thymidine uptake in non-Hodgkin's lymphoma using positron emission tomography. J. Nucl. Med., *29:* 1633–1637, 1988.

22. Shields, A. F., Mankoff, D. A., Link, J. M., Graham, M. M., Eary, J. F., Kozawa, S. M., Zheng, M., Lewellen, B., Lewellen, T. K., Grierson, J. R., and Krohn, K. A. Carbon-11-thymidine and FDG to measure therapy response. J. Nucl. Med., *39:* 1757–1762, 1998.

23. Van Eijkeren, M. E., De Schryver, A., Goethals, P., Poupeye, E., Schelstraete, K., Lemahieu, I., and De Potter, C. R. Measurement of short-term ^{11}C-thymidine activity in human head and neck tumours using positron emission tomography (PET). Acta Oncol., *31:* 539–543, 1992.

24. Young, H., Brock, C., Wells, P., and Price, P. Monitoring response to treatment in the development of anti-cancer drugs using positron emission tomography. Drug Inf. J., *33:* 237, 1999.

25. Conti, P. S., Alauddin, M. M., Fissekis, J. R., Schmall, B., and Watanabe, K. A. Synthesis of 2′-fluoro-5-[11C]-methyl-1-β-D-arabinofuranosyluracil ([11C]-FMAU): a potential nucleoside analog for *in vivo* study of cellular proliferation with PET. Nucl. Med. Biol., *22:* 783–789, 1995.

26. Bading, J. R., Shahinian, A. H., Bathija, P., and Conti, P. S. Pharmacokinetics of the thymidine analog 2′-fluoro-5-[14C]-methyl-1-β-D-arabinofuranosyluracil ([14C]-FMAU) in rat prostate tumor cells. Nucl. Med. Biol., *27:* 361–368, 2000.

27. Tjuvajev, J., Muraki, A., Ginos, J., Berk, J., Koutcher, J., Ballon, D., Beattie, B., Finn, R., Dahighian, F., and Blasberg, R. Iododeoxyuridine uptake and retention as a measure of tumor growth [published erratum appears in J. Nucl. Med., *34:* 1645, 1993]. J. Nucl. Med., *34:* 1152–1162, 1993.

28. Blasberg, R. G., Roelcke, U., Weinreich, R., Beattie, B., von Ammon, K., Yonekawa, Y., Landoit, H., Guenther, I., Crompton, N. E., Vontobel, P., Missimer, J., Maguire, R. P., Koziorowski, J., Knust, E. J., Finn, R. D., and Leenders, K. L. Imaging brain tumor proliferative activity with [^{124}I]iododeoxyuridine. Cancer Res., *60:* 624–635, 2000.

29. Grierson, J. R., and Shields, A. F. Radiosynthesis of 3′-deoxy-3′-[F-18]fluorothymidine: [F-18]FLT for imaging cellular proliferation *in vivo*. Nucl. Med. Biol., *27:* 143–156, 2000.

30. Grierson, J. R., Vesselle, H., Hofstrand, P., Chin, L., and Rasey, J. Comparative uptake and cell cycle measurements with [F-18]FLT vs [H-3]thymidine in mammalian tumor cells. J. Nucl. Med., *39:* 229, 1998.

31. Shields, A. F., Grierson, J. R., Dohmen, B. M., Machulla, H-J., Stayanoff, J. C., Lawhorn-Crews, J. M., Obradovich, J., Muzik, O., and Mangner, T. Imaging proliferation *in vivo* with [F-18]FLT and positron emission tomography. Nat. Med., *4:* 1334–1336, 1998.

32. Rasey, J. S., and Grierson, J. R. 3′-Deoxy-3′-[F-18]fluorothymidine predicts changes in cell proliferation. J. Nucl. Med. *40:* 25, 1999.

33. Rasey, J. S., Grierson, J. R., Wiens, L. W., and Kolb, P. E. Uptake of labeled FLT correlates with thymidine kinase (TK1) activity in human tumor cells. J. Nucl. Med., *41:* 36, 2000.

34. Schwartz, J. L., Grierson, J. R., Rasey, J. S., Wiens, L., Jordan, R., and Kohli, T. Rates of accumulation and retention of 3′-deoxy-3′-fluorothymidine (FLT) in different cell lines. J. Nucl. Med., *42:* 283, 2001.

35. Arner, E. S., Spasokoukotskaja, T., and Eriksson, S. Selective assays for thymidine kinase 1 and 2 and deoxycytidine kinase and their activities in extracts from human cells and tissues. Biochem. Biophys. Res. Commun., *188:* 712–718, 1992.

36. Langen, P., Etzold, G., Hintsche, R., and Kowollick, G. 3′-Deoxy-3′-fluorothymidine, a new selective inhibitor of DNA synthesis. Acta. Biol. Med. Ger., *23:* 759–766, 1969.

37. Matthes, E., Lehmann, C., Scholz, D., Rosenthal, H-A., and Langen, P. Phosphorylation, anti-HIV activity and cytotoxicity of 3′-fluorothymidine. Biochem. Biophys. Res. Commun., *153:* 825–831, 1988.

38. Munch-Petersen, B., Cloos, L., Tyrsted, G., and Eriksson, S. Diverging substrate specificity of pure human thymidine kinases 1 and 2 against antiviral dideoxynucleosides. J. Biol. Chem., *266:* 9032–9038, 1991.

39. Sherley, J. L., and Kelly, T. J. Regulation of human thymidine kinase during the cell cycle. J. Biol. Chem., *263:* 8350–8358, 1988.

40. Sundseth, R., Joyner, S. S., Moore, J. T., Dornsife, R. E., and Dev, I. K. The anti-human immunodeficiency virus agent 3′-fluorothymidine induces DNA damage and apoptosis in human lymphoblastoid cells. Antimicrob. Agents Chemother., *40:* 331–335, 1996.

41. Vesselle, H., Grierson, H., Muzi, M., Schmidt, R., Peterson, L. M., Pugsley, J., Vallières, E., Wood, D. E., and Krohn, K. A. ^{18}F-Fluorothymidine PET imaging of non-small cell lung cancer (NSCLC): comparison to Ki-67 proliferation index. J. Nucl. Med., *42:* 29, 2001.

42. Graham, M. M., and Lewellen, B. L. High-speed automated discrete blood sampling for positron emission tomography. J. Nucl. Med., *34:* 1357–1360, 1993.

43. Kohlmyer, S., Vesselle, H., Miyaoka, R., Kaplan, M., and Lewellen, T. Comparison of recovery coefficients for PET based on maximum and average ROI pixel values. Presented at the 2000 European Association of Nuclear Medicine Congress, Paris, Sept. 2–6, 2000.

44. Vesselle, H., Schmidt, R. A., Pugsley, J. M., Li, M., Kohlmyer, S. G., Vallières, E., and Wood, D. E. Lung cancer proliferation correlates with [F-18]fluorodeoxyglucose uptake by positron emission tomography. Clin. Cancer Res, *6:* 3837–3844, 2000.

45. Patlak, C., Blasberg, R., and Fenstermacher, J. Graphical evaluation of blood-to-brain transfer constants from multiple-time uptake data. J. Cereb. Blood Flow Metab., *3:* 1–7, 1983.

46. Key, G., Becker, M. H., Baron, B. Duchrow, M., Schluter, C., Flad, H. D., and Gerdes, J. New Ki-67-equivalent murine monoclonal antibodies (MIB 1–3) generated against bacterially expressed parts of the Ki-67 cDNA containing three 62 base pair repetitive elements encoding for the Ki-67 epitope. Lab Investig., *68:* 629–636, 1993.

47. Shields, A. F., Dohmen, B. M., Grierson, J. R., Kuntzsch, M., Machulla, H-J., and Bares, R. Imaging with [F-18]FLT and FDG in patients with cancer. J. Nucl. Med., *40:* 61, 1999.

48. Shields, A. F., Dohmen, B. M., Mangner, T. J., Lawhorn-Crews, J. M., Machulla, H., Muzik, O., and Bares, R. Imaging of thoracic tumors with [F-18]FLT. J. Nucl. Med., *41:* 74, 2000.

49. Dohmen, B. M., Shields, A. F., Dittman, H., Fersis, N., Eschmann, S. M., Philip, P., Reimold, M., Machulla, H. J., and Bares, R. Use of ^{18}FFLT for breast cancer Imaging. J. Nucl. Med., *42:* 29, 2001.

50. Shields, A. F., Dohmen, B. M., Mangner, T. J., Lawhorn-Crews, J., Machulla, H. J., Muzik, O., and Bares, R. Use of ^{18}F-FLT for imaging gastrointestinal tumors. J. Nucl. Med., *42:* 29, 2001.

51. Schwarting, R. Little missed markers and Ki-67. Lab. Invest., *68:* 597–599, 1993.

52. McCormick, D., and Hall, P. The complexities of proliferating cell nuclear antigen. Histopathology, *21:* 591–594, 1992.

53. Hall, P., Levinson, D., Woods, A. L., Yu, C. C., Kellock, D. B., Watkins, J. A., Barres, D. M., Gillett, C. E., Camplejohn, R., and Dover, R. Proliferating cell nuclear antigen (PCNA) immunolocalization in paraffin sections: an index of cell proliferation with evidence of deregulated expression in some neoplasms., J., Pathol., *162:* 285–294, 1990.

54. Gerdes, J., Lemke, H., Baisch, H., Wacker, H., Schwab, U., and Stein, H. Cell cycle analysis of a cell proliferation-associated human nuclear antigen defined by the monoclonal antibody Ki-67., J., Immunol., *133:* 1710–1715, 1984.

55. Schluter, C., Duchrow, M., Wohlenberg, C., Becker, M. H., Key, G., Flad, H. D., and Gerdes, J. The cell proliferation-associated antigen of antibody Ki-67: a very large, ubiquitous nuclear protein with numerous repeated elements, representing a new kind of cell cycle-maintaining proteins. J. Cell Biol., *123:* 513–522, 1993.

56. Scholzen, T., and Gerdes, J. The Ki-67 protein: from the known and the unknown. J. Cell Physiol., *182:* 311–322, 2000.

57. Rudolph, P., Peters, J., Lorenz, D., Schmidt, D., and Parwaresch, R. Correlation between mitotic and Ki-67 labeling indices in paraffin-embedded carcinoma specimens. Hum. Pathol., *29:* 1216–1222, 1998.

58. Cattoretti, G., Becker, M., Key, G., Duchrow, M., Schluter, C., Galle, J., and Gerdes, J. Monoclonal antibodies against recombinant parts of the Ki-67 antigen (MIB 1 and MIB 3) detect proliferating cells in microwave-processed formalin-fixed paraffin sections. J. Pathol., *168:* 357–363, 1992.

59. Toyohara, J., Kato-Azuma, M., Waki, A., Takamatsu, S., Yonekura, Y., Magata, Y., and Fujibayashi, Y. Basis of FLT as a cell proliferation marker: comparative uptake studies with thymidine, arabinothymidine and FDG, and cell-analysis in 22 asynchronously growing tumor cell lines. J. Nucl. Med., *42:* 83, 2001.

60. Arner, E. S. J., and Eriksson, S. Mammalian deoxyribonucleoside kinases. Pharmacol. Ther., *67:* 155–186, 1995.